fire

MDPI

Article

Experimental Study on the Influence of High-Pressure Water Mist on the Ceiling Temperature of a Longitudinally Ventilated Tunnel

Hui Zhu [1,*], Weining Du [1] and Wenfeng Li [2]

[1] Sichuan Fire Research Institute of MEM, Chengdu 610036, China; duweining@scfri.cn
[2] China Merchants Chongqing Communications Technology Research & Design Institute Co., Ltd., Chongqing 400067, China; liwenfeng@cmhk.com
* Correspondence: zhuhui@scfri.cn; Tel.: +86-15105217377

Abstract: In this study, a tunnel model with a length of 20 m, a width of 5 m, and a height of 5 m was used, and an experimental investigation was conducted to examine the impact of high-pressure water mist on the temperature distribution along the tunnel ceiling. Specifically, different experimental settings, such as various nozzle pressures, nozzle positions, and longitudinal ventilation speeds, in the high-pressure water mist system were employed to investigate the smoke-spreading process of tunnel fire under different conditions, and an effective method utilizing a high-pressure water mist system was proposed for blocking smoke and heat. The experimental results reveal that the high-pressure water mist system can be used to effectively improve the ceiling temperature during tunnel fires; when the nozzle pressure is set as 10 MPa, and the nozzle position is located at x7, the highest thermal insulation efficiency in the tunnel is obtained. Additionally, the joint application of the high-pressure water mist system and the mechanical smoke exhaust effectively mitigates the ambient temperature within the tunnel, thereby playing a pivotal role in enhancing the fire safety of the tunnel.

Keywords: tunnel fire; full-scale experiment; high-pressure water mist; thermal insulation; smoke barrier

Citation: Zhu, H.; Du, W.; Li, W. Experimental Study on the Influence of High-Pressure Water Mist on the Ceiling Temperature of a Longitudinally Ventilated Tunnel. *Fire* **2024**, *7*, 262. https://doi.org/10.3390/fire7080262

Academic Editor: Tiago Miguel Ferreira

Received: 21 June 2024
Revised: 14 July 2024
Accepted: 19 July 2024
Published: 23 July 2024

1. Introduction

China possesses an extensive and intricate topography, wherein mountainous regions in the central and western areas encompass approximately two-thirds of the total landmass. These mountainous terrains are abundant in forest resources, minerals, and other valuable assets. However, their accessibility remains a challenge. Consequently, the construction of highway tunnels and railway tunnels within these mountainous zones has emerged as a prudent choice from both economic and safety perspectives. According to statistics, the incidence rate of fire accidents in highway tunnels in China is $4/(10^8$ vehicles/km). With the increasing traffic flow in China, the incidence rate of tunnel fires has exceeded $15/(10^8$ vehicles/km), posing significant threats to both public and private assets as well as societal security. The primary danger of fires in tunnels mainly lies in the structural damage caused by elevated temperatures and the peril posed to trapped individuals due to smoke inhalation [1]. Therefore, research on tunnel fires has been widely conducted.

Some researchers have conducted pertinent experimental and numerical simulation studies on the efficacy of employing water mist curtains for smoke containment in tunnel fires. The research on water mist fire suppression technology was initiated in the 1940s and has progressively advanced alongside its expanding application domains. The influence of ventilation on the efficacy of water mist should be taken into account for applications involving natural or forced air circulation [2–4]. Dembele et al. [5] investigated the key factors affecting the thermal insulation effect of water curtains through experiments, including the size and density of water particles, the mole fraction of gas, and the width of

the water curtain. The results showed that smaller water particles exhibit superior thermal insulation properties [6,7]. Through theoretical and experimental research, Buchlin et al. [8] demonstrated the high efficacy of water curtains as protective measures for surrounding facilities in petrochemical and natural gas industries during oil tank fires. Additionally, vertical water curtains achieved a heat radiation-blocking effect ranging from 50 to 75%, while horizontal water curtains exhibited an impressive heat radiation-blocking effect of up to 90%. The European cost-effective, sustainable and innovative upgrading methods for fire safety in existing tunnels (UPTUN) project [9,10] proposed a water curtain separation system based on tunnel experimental reports. This system was used to divide smoke prevention zones, and a 20 MW fire experiment was conducted under longitudinal ventilation conditions. The experimental results showed that the upstream smoke prevention effect was satisfactory, while the downstream was ineffective. This indicates that the longitudinal airflow has a significant impact on the effectiveness of the water curtain for preventing smoke. Sun [11] and Li [12] conducted scaled tunnel experiments to explore the smoke and thermal insulation effects of fine water mist separation systems. The experimental findings demonstrated that, under natural ventilation conditions, the water mist separation system effectively impeded smoke propagation; however, it proved ineffective under longitudinal ventilation conditions. By using the FDS software (Version 5.0), Liang [13] constructed a 1:3 narrow and elongated spatial scale model test bench. The simulation results indicated that the water mist system can effectively manage fire and smoke while adequately regulating the ambient temperature within the tunnel to cater to personnel evacuation requirements. Nevertheless, Sun [11] and Li [12] conducted small-scale experiments with water mist pressure not exceeding 1 MPa. In contrast, Pan et al. [14] performed full-scale experiments in subway tunnels by installing fine water mist nozzles between platforms and tunnels. The results showed that the fine water mist system can effectively reduce the temperature of flue gas and the concentration of toxic gases. Amano [15] and Murakami [16] implemented a water curtain and water spray system in the tunnel, arranging the nozzles linearly to achieve fire separation and effectively prevent the spread of fire smoke. Based on the National Fire Protection Association (NFPA) 750 standard [17] for water mist fire suppression systems, water mist systems can be divided into low-pressure (working pressure $\leq$ 1.25 MPa), medium-pressure (working pressure 1.25 ~ 3.5 MPa), and high-pressure (working pressure $\geq$ 3.5 MPa) water mist systems.

In summary, there are few studies on the effectiveness of high-pressure water mist (working pressure $\geq$ 3.5 MPa) in controlling tunnel fire temperature under longitudinal ventilation conditions. Further research is needed to investigate the effectiveness of high-pressure water mist in controlling tunnel fire ceiling temperature and the interaction process between high-pressure water mist and tunnel fire smoke. Additionally, the heat and smoke insulation efficiency of high-pressure water mist and the influencing factors of the heat and smoke insulation efficiency are not clear, and a quantitative model describing the effect of a high-pressure water mist separation system is yet to be established. To this end, the effects of high-pressure water mist on tunnel ceiling temperature under longitudinal ventilation conditions were investigated through the full-scale 1:1 tunnel fire experiments. This study not only offers valuable insights into the development of an effective tunnel smoke control strategy, but also establishes a robust scientific foundation for tunnel fire protection design, fire prevention, and rescue measures.

2. Experimental Setup

2.1. Tunnel Geometry and Instrumentation

In the field of fire science, reduced-scale experiments and full-scale experiments are the commonly employed methodologies. Reduced-scale experiments refer to experiments with the reduced size and boundary conditions of the actual object in accordance with similarity principles of fluid mechanics. Reduced-scale experiments can be conducted in laboratories and offer greater control over conditions but fail to accurately capture the destructive impact of fire loads on experimental platforms when scaled up. Full-scale experiments

enable comprehensive observation of the specific performance of the research object under specified conditions and can even replicate fire scenarios. However, fire experiments are destructive experiments, and full-scale fire experiments can cause significant losses and are limited by site conditions and on-site control. To effectively reflect the real scene of tunnel fires, full-scale experiments were employed in this study.

The experimental platform for a 1:1 tunnel was established, measuring 20 m in length, 5 m in width, and 5 m in height. To accurately monitor the temperature distribution within the tunnel, eleven thermocouples were strategically positioned along its horizontal axis. These thermocouples were labeled as x-2, x-4, x-6, x-8, and x-10 in the upstream direction from the center position of the tunnel (x0), and as x2, x4, x6, x8, and x10 in the downstream direction. The values represent the distance from the center point of the fire source in meters. The thermocouple is installed in the upper left corner of the tunnel ceiling, 0.05 m away from the ceiling. To mitigate the impact of water on probes and minimize interference with temperature measurements, waterproof protection was implemented for all thermocouples in this experiment. The thermocouples were arranged within the channel to measure the temperature field of the tunnel fire, thereby capturing the initiation, progression, and propagation stages of fire development. The thermocouples with a diameter of 1 mm was employed to measure temperature, covering a temperature range of −50 to +800 °C. The fire source location was set at x0, and a set of fans was arranged at one end of the tunnel to investigate the variations in data during mechanical exhaust. Downstream of the tunnel, a camera was installed to document the progression of the fire. The experimental platform and test point layout are shown in Figure 1. In order to protect the tunnel structure in the experiment, rock wool board was installed on the tunnel wall for fire prevention. The characteristic parameters of rock wool board are shown in Table 1.

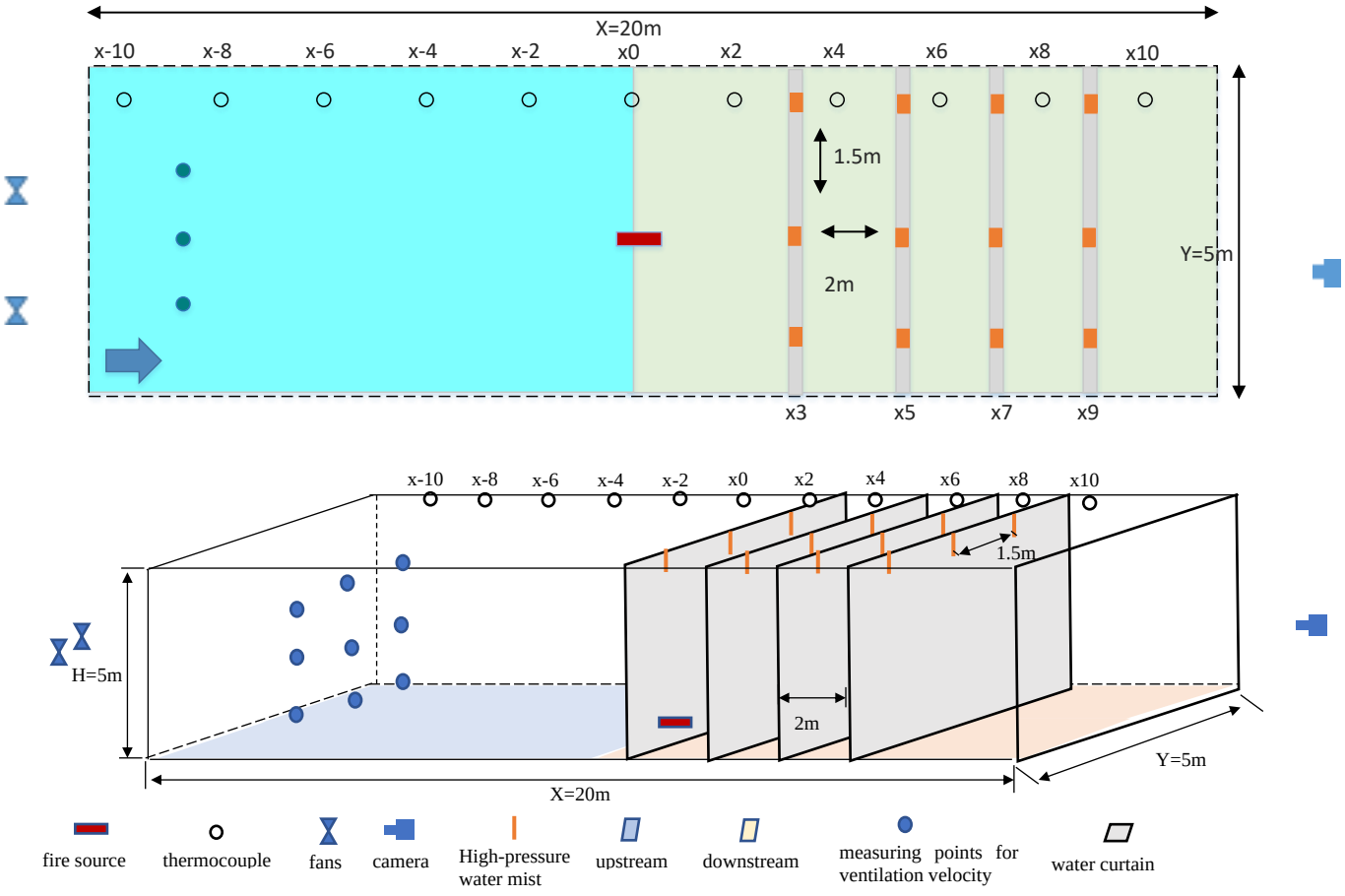

Figure 1. Layout of tunnel fire test platform and measuring points.

Table 1. Rock wool board characteristic parameters.

Material	Thickness (mm)	Thermal Conductivity/W/(m·K)	Specific Heat Capacity/kJ/(kg·K)	Density/kg/m^3
Rock wool board	50	0.039	750	150

2.2. High-Pressure Water Mist System

Figure 1 shows the installation diagram of the nozzle of the high-pressure water mist system. The ceiling downstream of the fire source is equipped with a total of 12 nozzles, arranged in four rows designated as x3, x5, x7, and x9. Each row consists of three nozzles. The spacing between the nozzles within each row is 1.5 m, while the spacing between adjacent rows is 2 m. Each nozzle is mounted near the ceiling and equipped with a separate valve to control its on/off state.

The pressure range of the high-pressure water mist system spanned from 0 to 12 MPa, with a motor power of 37 KW and a maximum flow rate of 150 L/min. In this experiment, the nozzle spray pressure was set at three levels: namely, 6 MPa, 8 MPa, and 10 MPa. The nozzle specification model was XSWT, and the nozzle flow coefficient was 0.5. The nozzle has 4 holes, each with a diameter of 1 mm. The spray droplet diameter $D_{v0.9} \leq 90$ µm. By using the flow calculation formula $q = K\sqrt{10P}$ [18], the flow rates of a single nozzle at pressures of 6 MPa, 8 MPa, and 10 MPa were determined to be 3.87 L/min, 4.47 L/min, and 5 L/min, respectively. Upon activation of the nozzle, a semi-circular water mist area will be sprayed out, as shown in Figure 2. Notably, the atomization cone angle of the nozzle is greater than 180°.

Figure 2. Schematic diagram of the experimental nozzle.

2.3. Heat Release Rate

N-heptane, a European standard fire source, was employed in this experiment to ensure high credibility and accuracy. The European standard fire serves as a benchmark for current fire research, and its various parameters hold significant importance in the field [19]. N-heptane is a liquid fuel characterized by stable combustion properties and experimental repeatability, possessing a theoretical calorific value of 4 466.6 kJ/mol (i.e., 100 g/mol, 44.666 MJ/kg) and a density of 0.68 kg/L [20].

The heat release rate is a fundamental parameter that governs the distribution of temperature and generation of smoke in a fire scenario. The accurate determination of this parameter forms the cornerstone of fire experiments. The oxygen consumption method [21–23] and the fuel weight loss method [23] are commonly used methods for measuring the heat release rate. In our experiment, the weight loss method was used to quantify the mass loss rate of n-heptane combustion, thereby obtaining the corresponding heat release rate. The following calculation equation is used [23]:

$$Q = \phi m_c \Delta H_c \quad (1)$$

where Q is the heat release rate, MW; ϕ is the combustion efficiency factor, which taken as 0.9 [20]; m_c is the instantaneous mass loss rate of the fuel, Kg/s; ΔH_c is the combustion but heat value, MJ/kg. The instantaneous mass loss rate of the fuel m_c can be obtained by differentiating the mass loss with respect to time. Due to periodic vibrations in the flames and plumes of pool fires during combustion, the instantaneous mass loss rate of the fuel will exhibit corresponding fluctuations. The instantaneous mass loss rate of the fuel can be calculated by Equation (2), with Δt set as 10 s.

$$m_c = \frac{m_t - m_{t+\Delta t}}{\Delta t} \quad (2)$$

The heat release rate (HRR) test of the fire source was conducted using a 2 m × 2 m square oil pan for a duration of 300 s. A total of 30 kg of n-hexane was used in each experiment. Table 2 shows a summary of the experimental conditions. The T1 series indicates no mechanical ventilation, while the T2 series indicates that mechanical ventilation is enabled. Figure 3 shows the mass loss curve for T1-1, T1-10, and T2-4.

Table 2. Summary of settings in different fire tests.

Test Number	Spray Nozzle Position	Ventilation Velocity (m/s)	Nozzle Pressure (MPa)	Average HRR (MW)
T1-1	NON	0	0	5.6
T1-2	x3	0	6	5.6
T1-3	x3	0	8	5.7
T1-4	x3	0	10	5.7
T1-5	x5	0	6	5.5
T1-6	x5	0	8	5.5
T1-7	x5	0	10	5.4
T1-8	x7	0	6	5.4
T1-9	x7	0	8	5.4
T1-10	x7	0	10	5.3
T1-11	x9	0	6	5.5
T1-12	x9	0	8	5.5
T1-13	x9	0	10	5.5
T2-1	NON	1.1	0	5.2
T2-2	NON	2.1	0	4.9
T2-3	x7	1.1	10	5.0
T2-4	x7	2.1	10	4.7

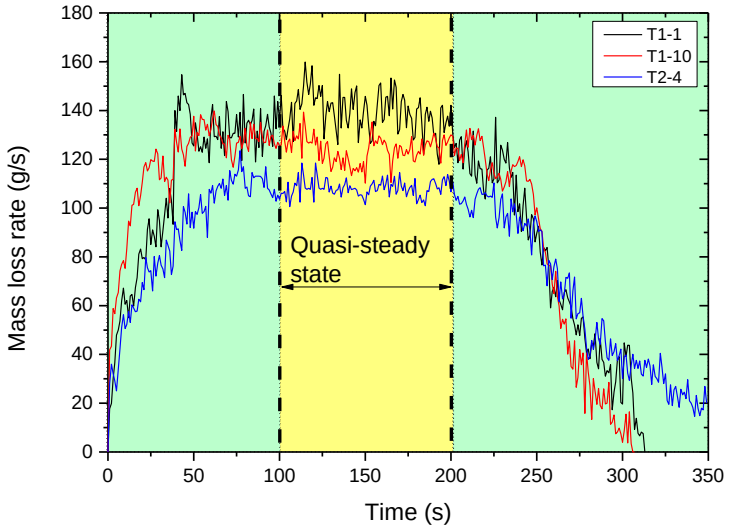

Figure 3. Mass loss rate diagram for T1-1, T1-10, and T2-4.

As shown in Figure 3, the curve development trend indicates that the mass loss rate initiates from a low value, undergoes a phase of growth, and subsequently stabilizes during a "quasi-steady-state period" spanning from 100 s to 200 s. Our study suggests that the time interval between 100 s and 200 s following ignition in this experiment represents the "quasi-steady-state period", wherein the tunnel fire maintains thermal equilibrium. Therefore, the heat release rate is determined during this period. Additionally, it can be found that, under the experimental conditions of mechanical smoke exhaust and high-pressure water mist system, the mass loss rate during fuel combustion is affected. This is because the temperature around the fire source decreases after the mechanical smoke exhaust and water curtain system is activated, resulting in a reduction in the thermal feedback of n-heptane and a reduction in mass loss. Sun et al. [11,12] reported that the heat release rate of a fire source decreases slightly under ventilation and water curtain conditions through experiments. The calculated heat release rate for experiment T1-1 is 5.6 MW, which can simulate the fire load of a small car burning [24]. Table 2 presents the calculated average HRR results for the remaining experimental conditions.

2.4. Longitudinal Ventilation System

The implementation of mechanical smoke extraction plays a crucial role in the management of smoke during tunnel fires. By integrating high-pressure water mist systems, the installation of mechanical smoke extraction fans upstream of the water curtain can effectively enhance the environmental conditions between the water curtain and the fire source [25]. In the experiment, two FZY-4E250 fans (power: 50 W, air volume: 1300 m^3/h) were positioned in front of the water curtain to effectively extract smoke. The smoke extraction rate was controlled by toggling the fans on and off. Nine measuring points were designated at the outlet section of the fan, and an anemometer was employed to measure and calculate the average wind speed at each point, as shown in Figure 1. In a longitudinal ventilation system, the critical wind speed is a crucial parameter that denotes the minimum longitudinal ventilation velocity required to prevent smoke from spreading upstream during a fire. According to the research conducted by Wu et al. [26], the critical wind speed can be calculated as follows:

$$\begin{cases} v^* = 0.4\left(\frac{Q^*}{0.20}\right)^{\frac{1}{3}}, Q^* \le 0.20 \\ v^* = 0.4, Q^* > 0.20 \\ Q^* = \frac{Q}{\rho_0 C_p T_0 g^{\frac{1}{2}} \overline{H}^{\frac{5}{2}}} \\ v^* = \frac{v_{cr}}{\sqrt{g\overline{H}}} \end{cases} \quad (3)$$

where $\overline{H}$ is the hydraulic diameter of the tunnel, $\overline{H} = 4A/P$, m; A is the cross-sectional area of the tunnel, m^2; P is the perimeter of the cross-section, m; v_{cr} is the critical wind speed; Q^* is the heat release rate during fire combustion, kW; ρ_0 is the air density, 1.2 kg/m^3; C_p is the specific heat capacity of air, 1 kJ/(kg·°C); T_0 is the ambient temperature and taken as 20 °C. Based on Equation (3), the theoretical critical wind speed V_{cr} of T1-1 ~ T2-4 falls within the range of 1.9 m/s and 2.1 m/s. Therefore, the longitudinal ventilation speeds of 1.1 m/s and 2.1 m/s for this experiment were selected for this experiment, which aligns with the findings reported by other researchers [27,28].

2.5. Summary of Test Settings

A total of 17 conditions were designed for this study, encompassing variables, such as nozzle pressure, nozzle position, and longitudinal ventilation. Each test was repeated three times for each scenario to obtain the most accurate data. In order to read data directly from the graph, the average value was drawn into the picture. The initial conditions and boundary conditions were carefully controlled to ensure consistency across all experimental scenarios. Given that the tunnel model was installed indoors, the natural ventilation conditions resulted in a negligible initial wind speed. Additionally, the ambient temperature

was maintained at 20 °C throughout the experiments. Table 2 shows a summary of the experimental conditions.

3. Experimental Results and Discussion

3.1. Analysis of the Impact of High-Pressure Water Mist on the Temperature of the Tunnel Ceiling under Natural Ventilation Conditions

3.1.1. Development Process of Tunnel Fire without a Water Curtain

Figure 4 shows the smoke spreading process in the tunnel under the experimental condition T1-1, with the initiation of combustion on the surface of the oil pool liquid serving as the reference time point. As depicted in Figure 4, after the ignition of the oil pool, a distinct layer of black smoke is formed at the upper part of the tunnel, while a ceiling jet flow spreads to both ends of the tunnel. The thickness of the smoke layer is calculated by the shadows on the wall. After 20 s, the smoke has spread throughout the tunnel. Following a flame development of 50 s, a stable smoke layer is developed and gradually descends. At about 70 s, the height of the smoke layer reaches approximately 2 m. With an increasing gas generation rate, a stable smoke layer (about 3 m in height) is essentially formed by 120 s and persists until the culmination of the entire combustion process. The experimental duration is approximately 300 s. As the tunnel constitutes an open space, it does not fill with smoke throughout the entire process of smoke settling. With regard to personnel evacuation safety, being situated at the end of the passage or in proximity to the location where smoke settles away from the fire source within the tunnel can be more hazardous. Smoke control measures should be implemented before the smoke layer reaches the average height of the evacuated crowd, which facilitates smoke elimination in a certain area and the safe evacuation of affected personnel.

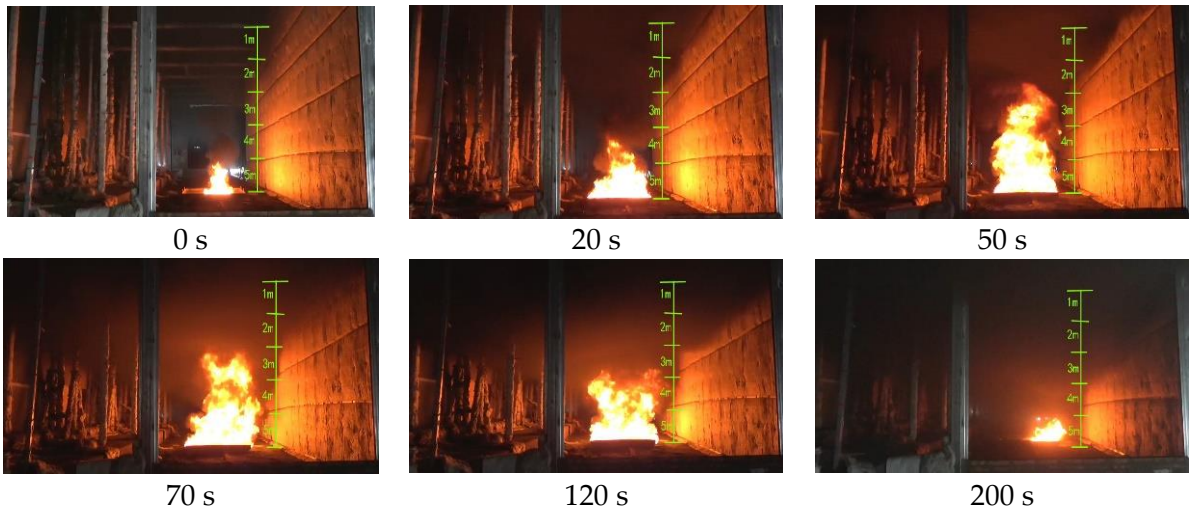

Figure 4. Smoke spread in the tunnel without a water curtain in experiment T1-1.

Figure 5 shows the time-varying curve of tunnel ceiling temperature in experiment T1-1. In the absence of a water curtain and mechanical smoke exhaust in experiment T1-1, the temperature change process can be divided into three stages: rapid development, stable transition, and attenuation reduction. This process reflects the sequential stages of fire propagation, starting from the ignition of the fire source and progressing towards stable combustion, followed by attenuation and eventual extinction. The uncontrolled spread and diffusion of smoke adhere to the regional model theory, characterized by a division into the hot smoke layer and the cold air layer. Consequently, this phenomenon results in rapid smoke accumulation throughout, significantly impeding personnel evacuation during fire incidents [29].

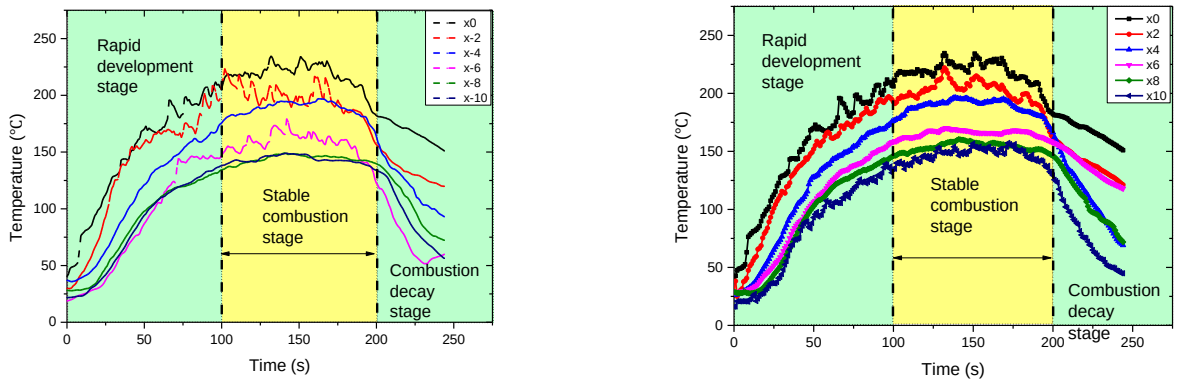

(**a**) upstream (**b**) downstream

Figure 5. Temporal variation of temperature in the tunnel ceiling under working condition T1-1.

As shown in Figure 5, the highest temperature (exceeding 230 °C) is concentrated at the central point of the fire source (x0). As one moves away from this origin in either direction, a gradual decrease in temperature can be observed. The temperature curves at x2 and x-2 exhibit similar characteristics, reaching a maximum temperature of about 215 °C. Similarly, the maximum temperature at x4 and x-4 is about 195 °C; it drops to about 165 °C at x6 and x-6; it further decreases to approximately 155 °C at x8 and x-8. Finally, the maximum recorded temperature stabilizes at around 150 °C at positions x10 and x-10. This observation suggests that, in the absence of any control measures, smoke disperses towards the ceiling and subsequently spreads to both ends. To further investigate the characteristics of the temperature field distribution in the tunnel without mechanical smoke extraction and water curtain systems, we compare the average temperature during the stable phase of fire combustion. Specifically, the average temperatures between 100 s and 200 s after the flame burns are considered, namely, the "quasi-steady-state period".

3.1.2. The Impact of Nozzle Pressure on the Temperature of the Tunnel Ceiling

The experiments T1-8, T1-9, and T1-10 were conducted to investigate the impact of varying nozzle spray pressures on the performance of the water mist segment system. The nozzle position was selected as position x7. The nozzle pressures were set as 6 MPa, 8 MPa, and 10 MPa, respectively, and experiment T1-1 was chosen as a reference for comparison. Figure 6 shows the average temperature distribution at the tunnel ceiling under the experimental conditions T1-8, T1-9, and T1-10. The stable combustion stage of the fire source was selected for analysis. As shown in Figure 6, the black dotted line represents the position (position x7) of water curtain separation. Upon activation of the water curtain system, a noticeable decrease in temperature was observed. In the absence of the water curtain, the temperature at the center of the fire source (x0) was 227 °C. However, with the initiation of the water curtain system, this value dropped to around 200 °C, indicating that the high-pressure water mist system possesses a cooling effect on the overall temperature of the tunnel. The vertical error bars for this set of the data indicate the range of levels in the three tests, and the error was not more than 8.2%.

As shown in Figure 6, there is a distinct temperature drop resembling a "cliff-like" pattern before and after the implementation of the water curtain system. Before its installation, the temperature at various temperature measurement points under different water curtain pressure conditions remains relatively consistent, with the temperature at x6 ranging between 145 and 150 °C. Following the introduction of the water curtain system, significant temperature changes are observed at these measurement points. When the water curtain pressure is 6 MPa, 8 MPa, and 10 MPa, the temperature at x8 is 75.6 °C, 66.4 °C, and 50.1 °C, respectively.

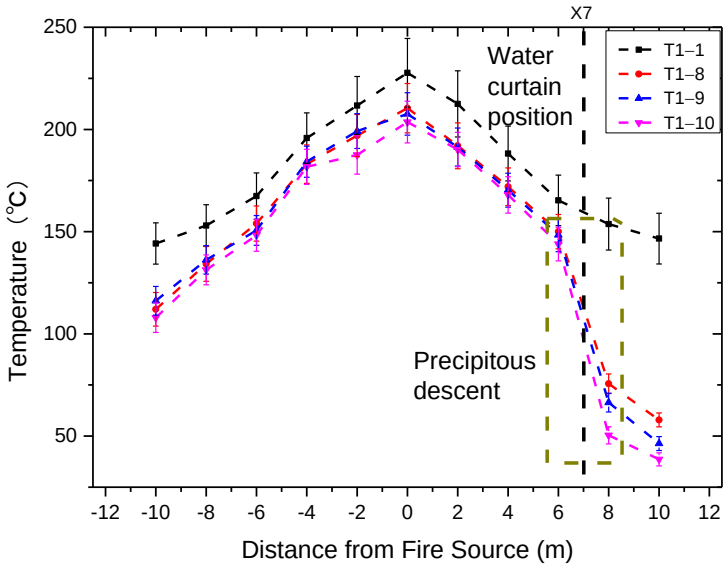

Figure 6. Temperature distribution of tunnel ceiling under different water spray pressures.

Under the identical fire source power and nozzle position, an increase in water spray pressure leads to a more pronounced cooling effect of the water curtain system and reduced smoke penetration through the surface, indicating that the high-pressure water mist exhibits superior smoke-proof capabilities. This can be attributed to the generation of smaller water particles and a higher particle count with the increased water spray pressure, thereby resulting in enhanced cooling efficiency. These findings align with the research conclusion by Sun et al. [11].

The comparison of the upstream and downstream temperatures of the fire sources in experiments T1-8, T1-9, and T1-10 (specifically at positions x-4 and x4) reveals a consistent observation, i.e., the upstream temperature surpasses that of the downstream. The main reason is that the high-pressure water mist system obstructs the upstream smoke, resulting in a higher upstream temperature compared to the downstream temperature. Additionally, the smoke temperature within the tunnel is lower than that in experiment T1-1 without a water curtain. This is because the activation of the water curtain system disrupts the original stratification of smoke, causing a certain degree of smoke deposition.

3.1.3. The Influence of the Nozzle Position on the Temperature of the Tunnel Ceiling

Experiments T1-4, T1-7, T1-10, and T1-13 were conducted to investigate the effect of different nozzle positions on the performance of the water mist segment system. In these experiments, the nozzle positions were set at x3, x5, x7, and x9, with a nozzle pressure of 10 MPa. Figure 7 shows the average temperature distribution from the ceiling position of the tunnel at the stable combustion stage of the fire source in experiments T1-4, T1-7, T1-10, and T1-13. It can be observed that the temperature exhibits a significant and abrupt decline resembling a "cliff-like" drop, both before and after the activation of the water curtain system at various nozzle positions, with an approximate temperature difference of 100 °C. The vertical error bars for this set of the data indicate the range of levels in the three tests, and the error was not more than 9.1%.

Further analysis reveals that the position of the sprinkler head directly affects the temperature distribution within the tunnel. The closer the sprinkler head is to the fire source, the higher the temperature in the tunnel. Taking experiment T1-4 as an example, the temperature prior to activating the water curtain system at position x3 is higher compared to that without a water curtain system in experiment T1-1 at the same measurement point. In experiment T1-1, the temperature at position x-2 is measured at 211.7 °C, while it reaches 217.6 °C in experiment T1-4. These findings suggest that the implementation of a water mist curtain system effectively mitigates downstream smoke propagation within the tunnel.

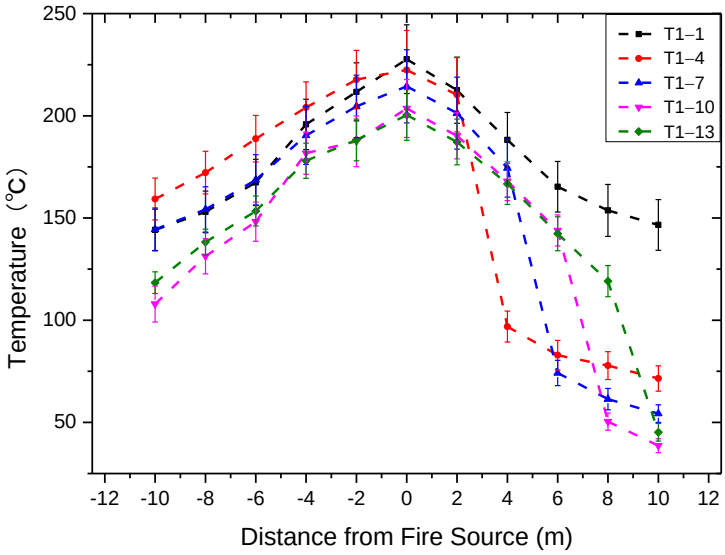

Figure 7. Temperature distribution of tunnel ceiling at different water spraying positions.

By comparing the upstream temperatures of experiments T1-4, T1-7, T1-10, and T1-13, it can be found that, as the nozzle proximity to the fire source increases, there is a corresponding elevation in the upstream temperature of the water curtain. The upstream smoke temperature in experiment T1-4 is higher than that in experiment T1-1, indicating that the high-temperature smoke spreading downstream is more likely to be blocked. However, the upstream temperatures of experiments T1-10 and T1-13 are comparable, indicating that nozzle position has negligible impact on upstream temperature when the distance between the nozzle and fire source point exceeds a certain threshold.

3.1.4. Discussion on the Thermal Insulation Efficiency of High-Pressure Water Mist under Natural Ventilation Conditions

During the process of smoke and heat resistance and cooling by fine water mist, a multitude of water droplets absorb the heat present in the smoke. These small water droplets, while moving within the high-temperature smoke, undergo convective heat transfer to elevate their own temperature and subsequently evaporate and gasify. Assuming that the water droplets are sufficiently minute with no internal temperature gradient, uniform internal temperature is maintained [30,31]. When a fire occurs in a tunnel, the longitudinal spread of fire smoke is effectively blocked by high-pressure fine water mist. On the cross section of the channel, there are uniform, dispersed and atomized fine water droplets. The high-speed movement of the water mist flow scours the carbon black particles in the fire smoke in the channel. Within the effective range of high-pressure fine water mist, its movement speed significantly surpasses that of the longitudinal smoke flow. Therefore, the relative velocity between the water droplets and carbon black particles can be approximated as the speed of movement of the water mist flow. In addition, it is assumed that the distribution of carbon black particles is uniform in the section where smoke flows [13].

The attenuation law of the temperature field on the downstream ceiling of a tunnel fire under natural ventilation conditions is firstly analyzed, followed by dimensional reduction of the temperature field [32]. Figure 8 shows the results of the non-dimensionalization process of the longitudinal temperature field attenuation of a fire. In this figure, ΔTx represents the average temperature rise at a distance x from the fire source, and $\Delta T0$ represents the average temperature rise of the thermocouple directly above the fire source at x0. It can be seen that under various experimental conditions, the dimensionless temperature experiences varying degrees of attenuation when smoke passes through a high-pressure water curtain. Notably, there is a significant decrease in the dimensionless temperature

on the protected side. However, the characteristics of dimensionless temperature gradient attenuation remain unclear for different nozzle positions and water curtain pressures.

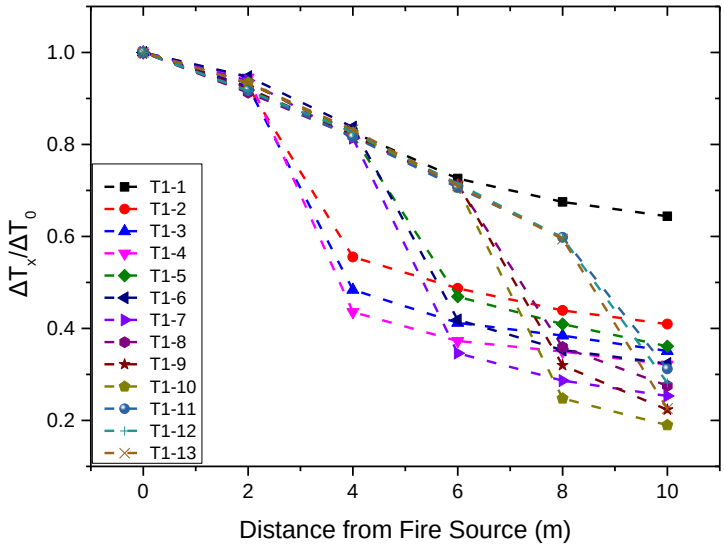

Figure 8. Dimensionless temperature distribution diagram of the downstream tunnel ceiling.

To facilitate the analysis of the thermal insulation efficiency of water curtains, the ratio of the dimensionless temperature drop before and after the implementation of the water curtain is used to characterize the thermal insulation ability of the water curtain. The heat attenuation of the water curtain is defined as the ratio of the dimensionless temperature difference before and after the implementation of the water curtain to the dimensionless temperature before the implementation of the water curtain:

$$\eta = \frac{\Delta T_x/\Delta T_0 - \Delta T_{x+2}/\Delta T_0}{\Delta T_x/\Delta T_0} \tag{4}$$

where η is the thermal insulation efficiency; $\Delta T_x/\Delta T_0$ is the dimensionless temperature before the implementation of water curtain; and $\Delta T_{x+2}/\Delta T_0$ is the dimensionless temperature after the implementation of water curtain.

Figure 9 shows the thermal insulation efficiency of high-pressure water mist. As depicted in the figure, the high-pressure water mist system exhibits a significantly elevated thermal insulation efficiency. In order to analyze the insulation efficiency of air, referring to Equation (4), the thermal insulation efficiency of the air is around 0.1. Upon activation of the high-pressure water mist system, the thermal insulation efficiency surpasses 0.4, and an increase in the working pressure of the nozzle further increases the thermal insulation efficiency. The reason for this phenomenon is that, as the nozzle pressure increases, the water spray flow per unit time increases, which improves the thermal insulation efficiency [33]. Simultaneously, it is evident that, as the nozzle position moves away from the fire point, there is an increase in thermal insulation efficiency. Taking a water pressure of 10 mpa as an example, when the nozzle positions are x3, x5, and x7, the thermal insulation efficiencies are measured at 0.54, 0.57, and 0.65, respectively. The comparison results show that there is a superior thermal insulation efficiency in experiment T1-10. However, once the water curtain position surpasses x7, a decline in thermal insulation efficiency can be observed.

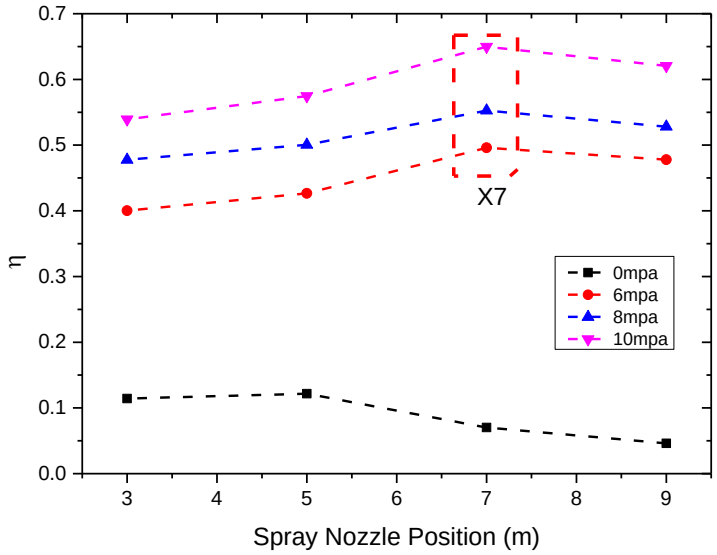

Figure 9. Thermal insulation efficiency of high-pressure water mist.

3.2. Analysis of the Impact of High-Pressure Water Mist on the Temperature of the Tunnel Ceiling under Mechanical Smoke Exhaust Conditions

3.2.1. Temperature Field Distribution in Tunnel under the Joint Action of Mechanical Smoke Extraction and High-Pressure Water Mist

Figure 10 shows the smoke spreading process within the tunnel under the experimental conditions of mechanical smoke extraction at a velocity of 2.1 m/s, water curtain positioned at x7, and water curtain pressure at 10 MPa in experiment T2-4. The zero-time point corresponds to the initiation of combustion on the surface of the oil pool liquid. As shown in Figure 10, upon ignition of the oil pool, a plume of black smoke is generated and accumulates at the tunnel's ceiling, forming a ceiling jet flow that diffuses towards both ends of the tunnel. After 20 s, the smoke has spread throughout the tunnel. As the combustion process progresses, the smoke quickly settles under mechanical smoke extraction conditions, and the smoke layer exceeds 3 m after 70 s; the smoke in the tunnel spills out from the water curtain section, and the high-pressure water curtain cannot effectively control the spread of fire smoke at 120 s. This indicates that a circumfluence is formed by smoke during mechanical ventilation, which has a certain impact on evacuation.

Figure 11 shows the time-varying curve of tunnel ceiling temperature in experiments T1-10 and T2-4; the temperature change include three stages: rapid development, stable transition, and attenuation reduction. Experiment T1-10 shows that the longitudinal ventilation speed is 0 m/s and T2-4 is 2.1 m/s, the nozzle position is at x7, and the nozzle pressure is 10 Mpa. It can be clearly seen from the figure that longitudinal ventilation can effectively reduce the temperature of flue gas downstream of the fire source. At position x0, the highest temperature of experiment T1-10 is about 200 °C, while T2-4 is 100 °C. At position x8 behind the water curtain, the highest temperature for both experiments was 50 °C.

To analyze the impact of mechanical smoke extraction on the temperature distribution characteristics of the tunnel, the average temperature at the ceiling position during the stable stage of fire combustion is selected for comparison. Figure 12 shows the longitudinal distribution of tunnel ceiling temperature at longitudinal wind speeds of 0 m/s, 1.1 m/s, and 2.1 m/s in experiments T1-1, T2-1, and T2-2. The vertical error bars for this set of the data indicate the range of levels in the three tests; the error was not more than 9.4%. It is evident that the activation of the mechanical smoke extraction system leads to an overall decrease in tunnel temperature. At the upstream location of the fire source, minimal temperature elevation occurs due to efficient ventilation, which effectively directs smoke downstream within the tunnel.

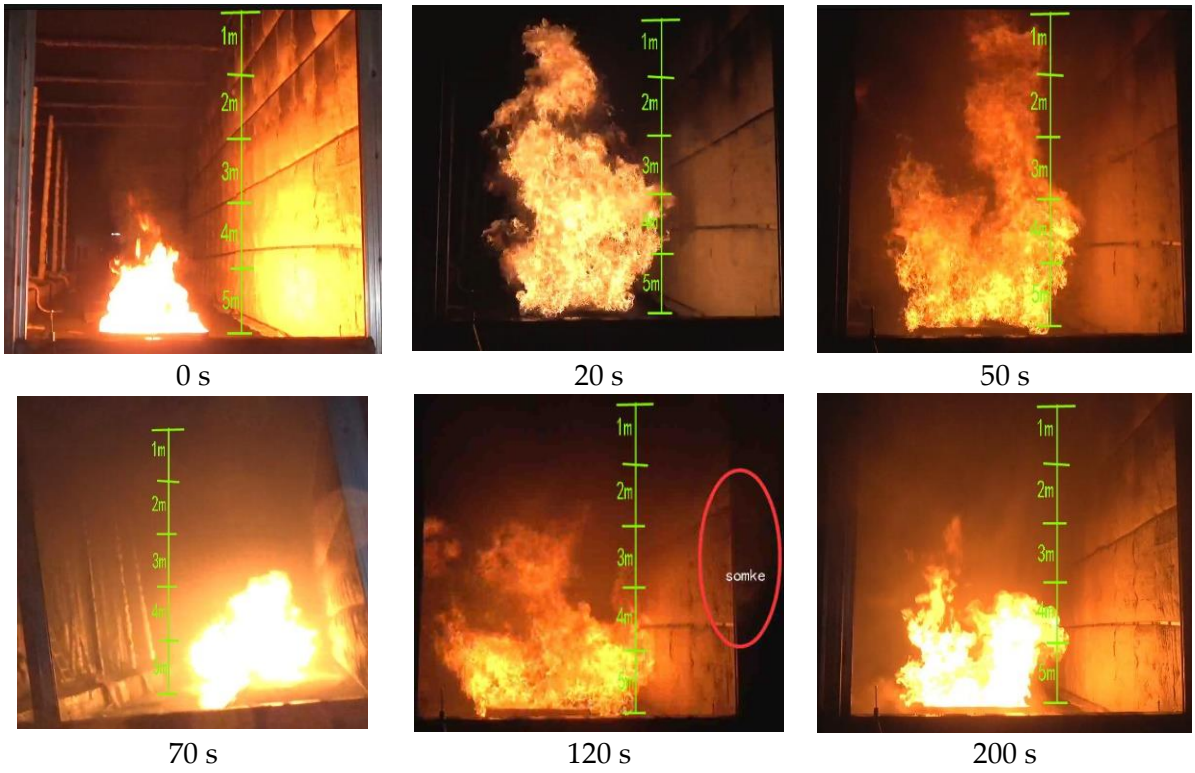

Figure 10. Smoke deposition process under the combined action of mechanical smoke extraction and high-pressure water mist in experiment T2-4.

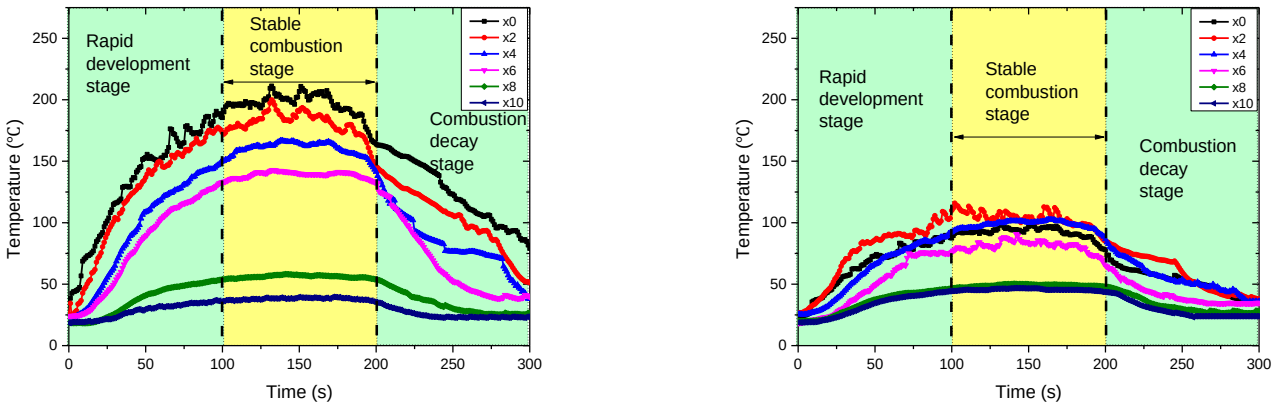

Figure 11. Temporal variation of temperature in the tunnel ceiling under working condition (**a**) T1-10 and (**b**) T2-4.

As the wind speed increases, the ceiling temperature decreases. At the center of the fire source x0, the temperature is measured as 227 °C without longitudinal ventilation, while it reduced to 181 °C with a longitudinal ventilation rate of 1.1 m/s, and further drops to 102 °C with a longitudinal ventilation of 2.1 m/s. The implementation of increased mechanical exhaust has proven to be effective in mitigating the upward transmission of temperature, resulting in a lower upstream temperature compared to the downstream temperature. Simultaneously, an increase in wind speed leads to a decrease in temperature near the fire area. For instance, when the longitudinal wind speed within the tunnel reaches 2.1 m/s, temperatures at x-4 upstream of the fire source remain below 50 °C, while temperatures at x10 downstream are already below 70 °C. As the wind speed increases, the

point of maximum temperature deviation shifts towards the downstream of the fire source, occurring approximately 2 m away from the center. The longitudinal wind speed inversely correlates with the temperature in the tunnel's downstream region, primarily attributed to enhanced ventilation-induced cooling effects.

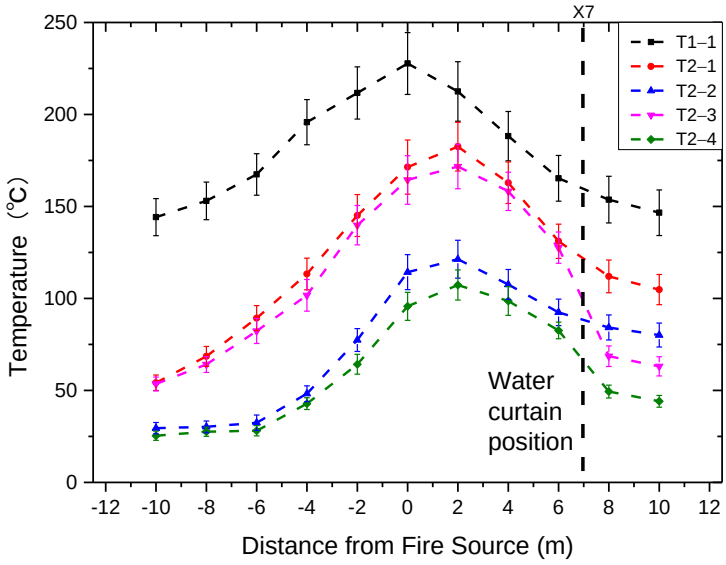

Figure 12. Longitudinal distribution of tunnel ceiling temperature under mechanical smoke extraction conditions.

The temperature distribution in the tunnel under the combined action of mechanical smoke extraction and high-pressure water mist in experiments T2-3 and T2-4 was further analyzed. In these experiments, the nozzle pressure was set as 10 MPa and nozzle position was located at position x7. Figure 12 shows the longitudinal distribution of the temperature field on the ceiling of the tunnel under the coupling condition of mechanical smoke extraction and high-pressure water curtain. It can be found that the lowest temperature is achieved due to the combined cooling effect of a high-pressure water mist system and mechanical smoke extraction. After passing through the high-pressure water curtain, the temperature of high-temperature smoke also decreases. When the wind speed is 1.1 m/s, the activation of the high-pressure water curtain results in a reduction of approximately 43.4 °C in temperature at x8. When the wind speed is 2.1 m/s, the implementation of the high-pressure water curtain leads to a decrease of about 34.8 °C in temperature at x8.

Even with the activation of a high-pressure water mist system, the downstream temperature in the protected area of a tunnel remains higher than the ambient temperature when mechanical smoke extraction is employed. However, in the presence of longitudinal ventilation, as long as the longitudinal wind speed exceeds the critical wind speed, the upstream spread of fire-generated smoke can be effectively prevented. The introduction of the longitudinal ventilation system induces the smoke to traverse the water mist screen system, facilitating a continuous exchange of heat between the smoke and surrounding droplets. Consequently, the heat carried by the smoke is incessantly absorbed by the droplets, leading to a reduction in temperature as it passes through the water mist screen system. Moreover, under strong longitudinal wind flow conditions, small-sized droplets will drift downstream with the wind current. Hence, even at locations distanced from the primary body of the water mist screen system, these small-sized droplets will still contribute to temperature reduction inside the tunnel through evaporation and heat absorption.

3.2.2. Discussion on the Thermal Insulation Efficiency under the Combined Action of Mechanical Smoke Extraction and High-Pressure Water Curtain

The attenuation law of the temperature field on the ceiling downstream of the tunnel fire is analyzed under conditions of mechanical smoke extraction, and a dimensional

reduction approach is applied to characterize the temperature field. Figure 13 shows the dimensionless treatment results of the longitudinal temperature field attenuation during a fire. In this figure, ΔTx represents the average temperature rise at a distance x from the fire source, while ΔT0 represents the average temperature rise of the thermocouple directly above the fire source at x0. It can be observed that, when mechanical smoke extraction is used in the tunnel, the longitudinal fire temperature field exhibits an initial increase followed by a subsequent decay, with the maximum dimensionless temperature occurring near x2. When high-pressure water mist is set at x7, there is a significant attenuation of the dimensionless temperature in experiments T2-3 and T2-4 at this location.

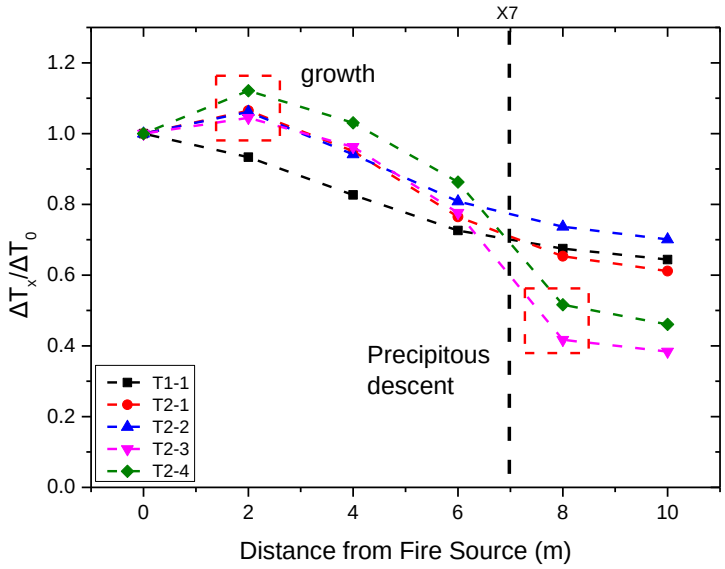

Figure 13. Dimensionless temperature distribution diagram of the downstream tunnel ceiling under mechanical smoke exhaust conditions.

The thermal insulation efficiency of high-pressure water mist under mechanical smoke extraction conditions is further explored by using the ratio of the dimensionless temperature drop before and after the application of high-pressure water mist, and the thermal insulation capability of water curtains is obtained. The thermal insulation efficiency under mechanical smoke exhaust conditions is calculated by Equation (4) and compared with the thermal insulation efficiency under non-mechanical smoke exhaust conditions, as shown in Figure 14. When the mechanical smoke extraction system is integrated to the high-pressure water mist system, the thermal insulation efficiencies in experiments T2-3 and T2-4 are 0.462 and 0.412, respectively. Compared to experiment T1-2, the thermal insulation efficiencies in experiments T2-3 and T2-4 are higher than those in experiment T1-2 with a single high-pressure water mist system. Comparing experiments T1-10, T2-3, and T2-4, it can be observed that the higher pressure of water mist brings higher thermal insulation efficiency, but the combination of higher ventilation velocity and higher pressure of water mist decreases the insulation efficiency. Therefore, the integration of a high-pressure water mist system with the mechanical smoke exhaust system is feasible in engineering applications. The mechanical smoke exhaust system effectively reduces the flue gas temperature upstream of the fire source, while the high-pressure water mist system reduces the flue gas temperature downstream of the fire source.

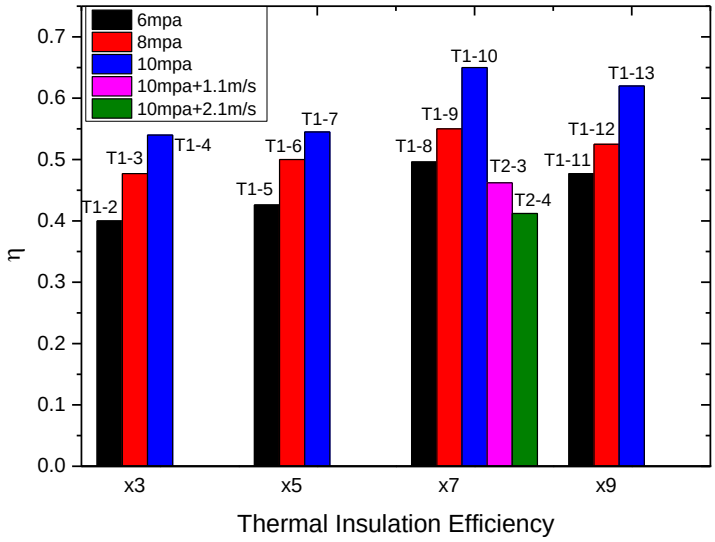

Figure 14. Comparison of thermal insulation efficiencies in different experiments.

4. Conclusions

In a 1:1 tunnel model with a length of 20 m, a width of 5 m, and a height of 5 m, a field test was conducted to investigate the effectiveness of high-pressure water mist suppression on ceiling temperature. A series of 17 tests were conducted with varying settings, including nozzle pressure, nozzle position, and longitudinal ventilation speed. This study provides insights into the smoke spread process during tunnel fires under different conditions and discusses the temperature distribution in these scenarios. The conclusions are drawn as follow:

(1) During natural ventilation, the cooling effect of the water curtain system becomes more pronounced with increasing water spray pressure. A reduced amount of smoke passing through the water curtain indicates an enhanced smoke-blocking efficacy of the high-pressure water mist. The position of the nozzle directly affects the temperature distribution within the tunnel. The closer the nozzle position is to the fire source, the higher the temperature upstream of the high-pressure water mist system. With a nozzle pressure set at 10 MPa and positioned at x7, optimal thermal insulation efficiency can be achieved.

(2) When the mechanical smoke evacuation system is activated, it leads to a reduction in the overall temperature within the tunnel. Increasing mechanical ventilation is effective in mitigating the upstream spread of smoke temperature, with upstream temperatures lower than downstream temperatures. The greater the longitudinal wind speed, the lower the temperature downstream of the tunnel. The maximum temperature in the tunnel occurs near position x2. The smoke from fire cannot be effectively blocked by the high-pressure water mist system, and its heat resistance efficiency is lower compared to natural ventilation.

(3) When the mechanical smoke extraction system is integrated with the high-pressure water mist system, the higher thermal insulation efficiencies of experiments T2-3 and T2-4 (0.462 and 0.412) can be obtained compared to those in experiment T1-2 with a single high-pressure water mist system. Therefore, it is feasible to integrate the high-pressure water mist system with the mechanical smoke exhaust system in engineering applications.

In summary, the high-pressure water mist system can effectively improve the ceiling temperature in tunnel fires. Although solely relying on the high-pressure water mist system cannot permanently obstruct smoke, it can efficiently impede hot smoke within a specific range. Moreover, the integration of the high-pressure water mist system with mechanical smoke exhaust effectively mitigates the tunnel ambient temperature, thereby playing a

pivotal role in enhancing tunnel fire safety performance. However, the research content has the following limitations. Firstly, the tunnel length is only 20 m, and the experiment only recorded the temperature field near the fire source. Secondly, a single power fire source is used in the experiment, and there is no standard experiment. Thirdly, in tunnel fires, the smoke layer is damaged due to the suction effect of high-pressure water mist, and the height of the smoke layer directly affects the safety of personnel evacuation. Therefore, the authors' next step will be to build a longer tunnel model, conduct experiments on the heat release rate of fire sources under standard conditions, analyze the distribution characteristics of smoke temperature in the tunnel along the height direction, and establish a theoretical model based on the experimental data.

Author Contributions: Conceptualization, H.Z. and W.D.; methodology, H.Z.; investigation, H.Z. and W.L.; writing—original draft preparation, H.Z.; writing—review and editing, H.Z.; supervision, H.Z.; funding acquisition, H.Z. and W.L.; All authors have read and agreed to the published version of the manuscript.

Funding: This work was supported by the Sichuan Science and Technology Program (2023YFS0427), National Key R&D Program of China (2021YFC3002000) and (2021YFC3002002-2), Sichuan Fire Research Institute of MEM Science and Technology Projects (20248815Z), and the Natural Science Foundation of Chongqing Municipality (CSTB2022NSCQ-MSX1049).

Institutional Review Board Statement: Not applicable.

Informed Consent Statement: Not applicable.

Data Availability Statement: Data are contained within the article.

Conflicts of Interest: Author Wenfeng Li was employed by the company China Merchants Chongqing Communications Technology Research & Design Institute Co., Ltd. The remaining authors declare that the research was conducted in the absence of any commercial or financial relationships that could be construed as a potential conflict of interest.

References

1. Zhang, Y.; Huang, X. A Review of Tunnel Fire Evacuation Strategies and State-of-the-Art Research in China. *Fire Technol.* **2022**, *60*, 859–892. [CrossRef]
2. Back, G.G. An overview of water mist fire suppression system technology. In Proceedings of the Halon Alternatives Technical Working Conference, Albuquerque, NM, USA, 11–13 May 1994.
3. Lemaire, T.; Kenyon, Y. Large scale fire tests in the Second Benelux Tunnel. *Fire Technol.* **2006**, *42*, 329–350. [CrossRef]
4. Li, Y.Z.; Ingason, H. Position of Maximum Ceiling Temperature in a Tunnel Fire. *Fire Technol.* **2014**, *50*, 889–905. [CrossRef]
5. Dembele, S.; Wen, J.X.; Sacadura, J.F. Experimental Study of Water Sprays for the Attenuation of Fire Thermal Radiation. *J. Heat Transf.* **2001**, *123*, 534–543. [CrossRef]
6. Gupta, M.; Pasi, A.; Ray, A.; Kale, S.R. An experimental study of the effects of water mist characteristics on pool fire suppression. *Exp. Therm. Fluid Sci.* **2013**, *44*, 768–778. [CrossRef]
7. Gupta, M.; Rajora, R.; Sahai, S.; Shankar, R.; Ray, A.; Kale, S.R. Experimental evaluation of fire suppression characteristics of twin fluid water mist system. *Fire Saf. J.* **2012**, *54*, 130–142. [CrossRef]
8. Buchlin, J.M. Thermal shielding by water spray curtain. *J. Loss Prev. Process Ind.* **2005**, *18*, 423–432. [CrossRef]
9. Hejny, H. *The European Project UpTun: Results of Four Years of Research to Improve the Level of Fire Safety in Existing Tunnels*; WIT Press: Billerica, MA, USA, 2007.
10. McCory, T.; Sprakel, D.; Christensen, E. Engineering Guidance for Water Based Fire Fighting Systems for the Protection of Tunnels and Subsurface Facilities, WP2 Fire Development and Mitigation Measures D251. UPTUN. 2008. Available online: https://uptun.net/ (accessed on 13 July 2024).
11. Sun, J.; Fang, Z.; Tang, Z.; Beji, T.; Merci, B. Experimental study of the effectiveness of a water system in blocking fire-induced smoke and heat in reduced-scale tunnel tests. *Tunn. Undergr. Space Technol.* **2016**, *56*, 34–44. [CrossRef]
12. Li, Q.; Tang, Z.; Fang, Z.; Yuan, J.; Wang, J. Experimental study of the effectiveness of a water mist segment system in blocking fire-induced smoke and heat in mid-scale tunnel tests. *Tunn. Undergr. Space Technol.* **2019**, *88*, 237–249. [CrossRef]
13. Liang, Q.; Li, Y.; Li, J.; Xu, H.; Li, K. Numerical studies on the smoke control by water mist screens with transverse ventilation in tunnel fires. *Tunn. Undergr. Space Technol.* **2017**, *64*, 177–183. [CrossRef]
14. Pan, L.W.; Lo, S.M.; Liao, G.X. Experimental study of smoke control in subway station for tunnel area fire by water miss system. *Procedia Eng.* **2011**, *11*, 335–342.

15. Amano, R. *Applicability of Water Screen Fire Disaster Prevention System to Roadtunnels in Japan*; Tunnel Safety and Ventilation: Graz, Austria, 2006; pp. 162–173.
16. Murakami, M.; Kurioka, H.; Imazeki, O.; Kuwana, H.; Amano, R. Numerical Simulation in Effect of Compartmentalization with Water Screen (WS) in a Tunnel Fire. *Seisan Kenkyu* **2007**, *59*, 313–317.
17. NFPA. *Standard on Water Mist Fire Protection Systems*; NFPA: Boston, MA, USA, 2000.
18. *China SPo. GB 50898*; Technical Code for Water Mist Fire Extinguishing System. Ministry of Housing and Urban-Rural Development of the People's Republic of China: Beijing, China, 2013.
19. Lin, C.H.; Ferng, Y.M.; Hsu, W.S.; Pei, B.S. Investigations on the Characteristics of Radiative Heat Transfer in Liquid Pool Fires. *Fire Technol.* **2010**, *46*, 321–345. [CrossRef]
20. Roh, J.S.; Yang, S.S.; Hong, S.R.; Yoon, M.O.; Jeong, Y.T. An experimental study on the effect of ventilation velocity on burning rate in tunnel fires—Heptane pool fire case. *Build. Environ.* **2008**, *43*, 1225–1231. [CrossRef]
21. *ISO9705*; Fire Tests—Full-Scale Room Test for Surface Products. ISO: Geneva, Switzerland, 1993.
22. Huggett, C. Estimation of rate of heat release by means of oxygen consumption measurements. *Fire Mater.* **1980**, *4*, 61–65. [CrossRef]
23. Quintiere, J.G. *Fundamentals of Fire Phenomena*; John Wiley & Sons Ltd.: Hoboken, NJ, USA, 2006.
24. Zhu, H.; Gao, Y.; Guo, H. Experimental investigation of burning behavior of a running vehicle. *Case Stud. Therm. Eng.* **2020**, *22*, 100795. [CrossRef]
25. Hu, L.H.; Huo, R.; Peng, W.; Chow, W.K.; Yang, R.X. On the maximum smoke temperature under the ceiling in tunnel fires. *Tunn. Undergr. Space Technol.* **2006**, *21*, 650–655. [CrossRef]
26. Wu, Y.; Bakar, M.Z.A. Control of smoke flow in tunnel fires using longitudinal ventilation systems—A study of the critical velocity. *Fire Saf. J.* **2000**, *35*, 363–390. [CrossRef]
27. Kazemipour, A.; Afshin, H.; Farhanieh, B. A Comprehensive Study on the Critical Ventilation Velocity in Tunnels with Different Geometries. *Int. J. Vent.* **2015**, *14*, 303–319. [CrossRef]
28. Li, Y.Z.; Fan, C.G.; Ingason, H.; Lönnermark, A.; Ji, J. Effect of cross section and ventilation on heat release rates in tunnel fires. *Tunn. Undergr. Space Technol.* **2016**, *51*, 414–423. [CrossRef]
29. Hu, L.H.; Li, Y.Z.; Huo, R.; Yi, L.; Chow, W.K. Full-scale experimental studies on mechanical smoke exhaust efficiency in an underground corridor. *Build. Environ.* **2006**, *41*, 1622–1630. [CrossRef]
30. Morgan, H.P.; Baines, K. Heat transfer from a buoyant smoke layer beneath a ceiling to a sprinkler spray. 2—An experiment. *Fire Mater.* **1979**, *3*, 34–38. [CrossRef]
31. Zhu, H.; Zhu, G.; Gao, Y.; Zhao, G. Experimental Studies on the Effects of Spacing on Upward Flame Spread over Thin PMMA. *Fire Technol.* **2016**, *53*, 673–693. [CrossRef]
32. Zhu, H.; Ji, J.; Nie, J. Early fire evolution and alarm characteristics of cable fires in long and narrow spaces. *Fire Saf. J.* **2022**, *131*, 103627. [CrossRef]
33. Tang, Z.; Fang, Z.; Yuan, J.P.; Merci, B. Experimental study of the downward displacement of fire-induced smoke by water sprays. *Fire Saf. J.* **2013**, *55*, 35–49. [CrossRef]